ACS APPLIED MATERIALS & INTERFACES

Letter

www.acsami.org

Upconversion-Agent Induced Improvement of g-C_3N_4 Photocatalyst under Visible Light

Jingsan Xu,[†] Thomas J. K. Brenner,[‡] Zupeng Chen,[†] Dieter Neher,[‡] Markus Antonietti,[†] and Menny Shalom*,[†]

[†]Department of Colloid Chemistry, Max Planck Institute of Colloids and Interfaces, 14424 Potsdam, Germany

[‡]Institute of Physics & Astronomy, University of Potsdam, 14476 Potsdam, Germany

Supporting Information

ABSTRACT: Herein, we report the use of upconversion agents to modify graphite carbon nitride (g-C_3N_4) by direct thermal condensation of a mixture of $ErCl_3{\cdot}6H_2O$ and the supramolecular precursor cyanuric acid-melamine. We show the enhancement of g-C_3N_4 photoactivity after Er^{3+} doping by monitoring the photodegradation of Rhodamine B dye under visible light. The contribution of the upconversion agent is demonstrated by measurements using only a red laser. The Er^{3+} doping alters both the electronic and the chemical properties of g-C_3N_4. The Er^{3+} doping reduces emission intensity and lifetime, indicating the formation of new, nonradiative deactivation pathways, probably involving charge-transfer processes.

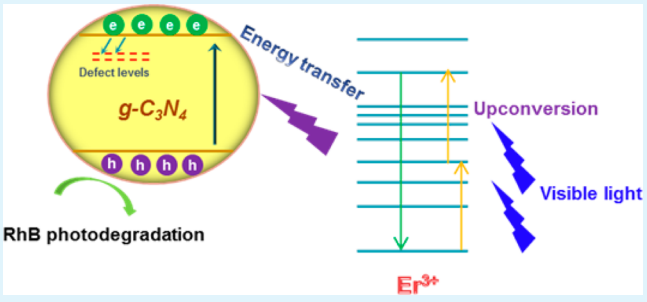

KEYWORDS: *metal-free photocatalysis, upconversion, carbon nitride, RhB photodegradation*

Photocatalysis based on semiconductors attracts great attention because of its high potential in energy and environmental related fields, such as hydrogen/oxygen evolution by water splitting,[1] oxidizing organic pollutants,[2] reduction of carbon dioxide,[3,4] etc. The semiconductor absorbs photons with higher energies than its bandgap and generates electron−hole pairs that are able to drive the desired reactions. In general, most of the semiconductor photocatalysts consist of one metal center (transition-metal ion or post-transition-metal ion), e.g., the well-known TiO_2,[5] Fe_2O_3,[6] $BiVO_4$,[7] and others.[8] In 2009, it was found that a metal-free semiconductor, graphitic carbon nitride (g-C_3N_4), can efficiently split water to hydrogen and oxygen under visible light.[9] This air-stable, cheap, and nontoxic material immediately attracted wider interest and has meanwhile also been demonstrated to show high performance in the fields of electrocatalysis,[10,11] heterogeneous catalysis,[12] and photocatalysis.[13] Several strategies such as element doping,[14] chemical modifications,[15,16] morphology control,[17] and material combinations[18−20] have been employed to modify g-C_3N_4 for better light harvesting. Recently, a supramoleculer-precursor approach was proposed in order to template photoactive g-C_3N_4 by two groups,[21,22] which used a preorganized cyanuric acid-melamine (CM) complex as the starting material. However, it remains crucial to broaden the light absorption of g-C_3N_4 because of its wide band gap of ∼2.7 eV.[13]

Upconversion luminescence is a unique optical process whereby low-energy photons can be converted to high-energy photons, which is contrary to conventional luminescence phenomena. So far lanthanide ions show the best activity as upconversion agents, because they have many available states in the IR to visible range with relatively long lifetimes, which is favorable for the upconversion process.[23] With the ability to allow wavelength transformation, upconversion materials have been used in a variety of fields, such as lasers, optoelectronic devices[24] and especially in bioimaging over the past few years.[25] Upconversion agents were introduced to photocatalysis as well, either by direct doping or by making hybrids.[26,27] This strategy enables photocatalysts to overcome their theoretical conversion efficiency by harvesting also photons with lower energies than their bandgap.

Herein, we used erbium and thulium ions as upconversion agents to modify the photocatalytic activity of g-C_3N_4. The influence of the rare-earth element doping concentration on the chemical and optoelectronic properties of g-C_3N_4 was studied. RhB photodegradation under visible light was conducted to evaluate the extended photoactivity of doped g-C_3N_4. In addition, the contribution of upconversion effects was confirmed by the photodegradation under red light laser.

The Er^{3+} doped g-C_3N_4 was prepared by an in situ synthesis approach. Briefly, a defined amount of $ErCl_3{\cdot}6H_2O$ (molar ratio relative to the matrix) was mixed with the cyanuric acid-melamine supramoleculer precursor by grinding, and the mixture was transferred to the furnace and annealed at 550 °C in N_2 flow for 4 h. In the cases of low Er^{3+} amount (up to

Received: August 1, 2014
Accepted: September 19, 2014
Published: September 19, 2014

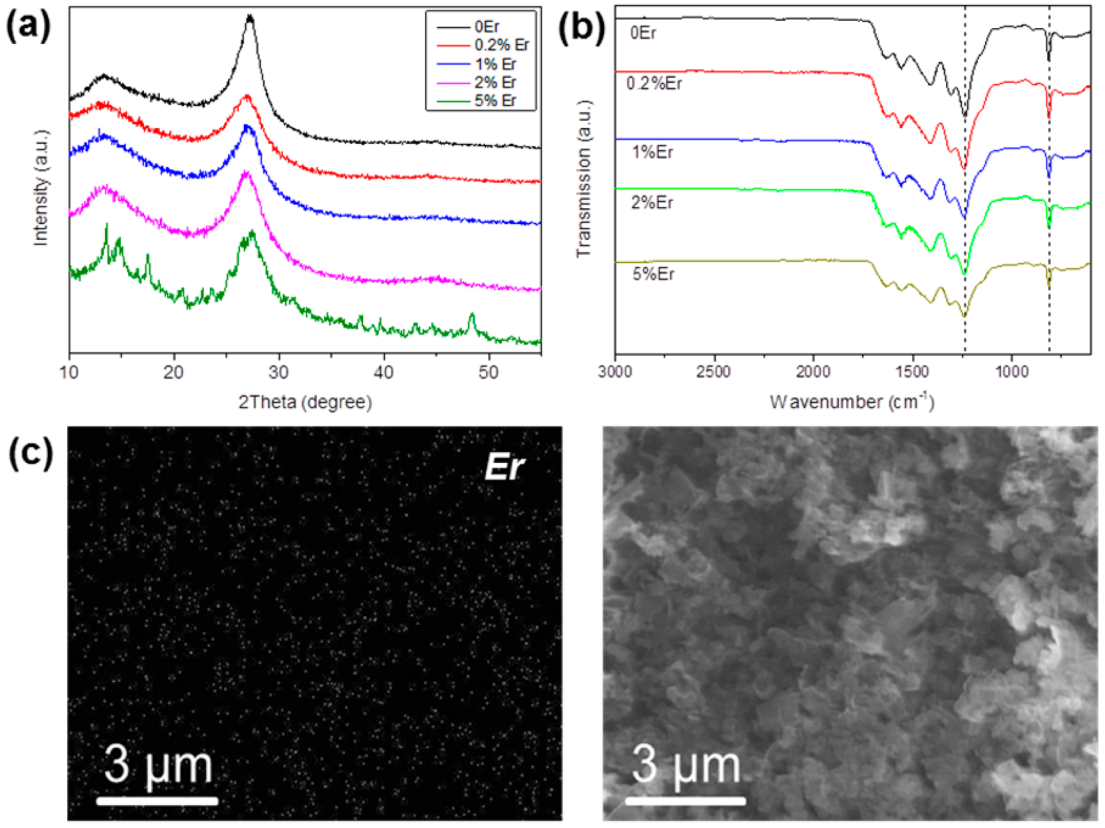

Figure 1. (a) XRD patterns and (b) FTIR spectra of g-C_3N_4 with different Er^{3+} doping amount. (c) Er EDX mapping (left) and corresponding SEM image (right) of 2% Er^{3+} doped g-C_3N_4.

2%), the X-ray diffraction (XRD) patterns of doped materials (Figure 1) show only diffraction features of g-C_3N_4. The strong peak at around 27° is from the interplanar stacking of the aromatic system, and the broad one at 13° is attributed to in-plane repeat units. $ErCl_3{\cdot}6H_2O$ diffraction peaks in final hybrid start to appear when the doping concentration reached 5%, indicating that the sample probably turned into a composite of g-C_3N_4 and $ErCl_3{\cdot}6H_2O$. This however also supports our concept that Erbium essentially stays in the form of the trivalent chloride and is neither reduced to metallic Erbium nor converted into the corresponding nitride. We note that $ErCl_3{\cdot}6H_2O$ can transform to tetragonal ErOCl at high temperature; however, our results show that in the presence of the CM complex, only the diffraction peaks from $ErCl_3{\cdot}6H_2O$ can be observed (see Figure S1 in the Supporting Information).

g-C_3N_4 formation is further confirmed by Fourier transform infrared (FTIR) spectra as shown in Figure 1b. The typical stretching modes of C−N heterocycles located at 1200−1600 cm^{-1} are observed, along with the vibration peak at 812 cm^{-1}, which is the characteristic absorption peak of the triazine unit. It is important to note that all the Er^{3+} doped g-C_3N_4 samples do not show any observable shift (dashed lines) or additional vibration modes in the FTIR spectrum, indicating that the introduction of Er^{3+} has almost no effect on the bonding or packing of the g-C_3N_4 structures.[15] Moreover, scanning electron microscopy (SEM) images (see Figure S2 in the Supporting Information) show that low amounts of Er^{3+} do not have much impact on the morphology of g-C_3N_4. In addition, energy-dispersive X-ray (EDX) spectroscopy mapping (Figure 1c) demonstrates that Er^{3+} (2%) ions are uniformly dispersed in the g-C_3N_4 matrix, presumably together with their chlorine-counterions. Additional EDX mappings for carbon, nitrogen, and chlorine are given in Figure S3 in the Supporting Information. The Er^{3+} ions can be incorporated into the nitride pores of the g-C_3N_4 structure built by triazine or tri-s-triazine units.[28] There is also possibility that Er^{3+} ions have strong electrostatic interaction with g-C_3N_4, given that pristine g-C_3N_4 is highly negatively charged with a zeta potential of −46 mV, whereas 2%Er−C_3N_4 is basically electrically neutral and no stable colloid can be produced (see Figure S4b in the Supporting Information). The schematical structure of Er^{3+}-doped g-C_3N_4 is shown in Figure S4a in the Supporting Information.

Figure 2a shows the UV−vis absorption spectra of the g-C_3N_4 with different Er^{3+} content. All the g-C_3N_4 samples show an absorption edge of 460 nm, corresponding to a bandgap of 2.7 eV. For the lowest Er^{3+} doping concentration (0.2%) tested here, the product already shows a weak but clear absorption peak at 522 nm (inset of Figure 2a), arising from the transition to the levels $^4S_{3/2}$−$^2H_{11/2}$ in Er^{3+}. With increasing Er^{3+} amount, additional absorption peaks at 654, 487, and 800 nm which correspond to transitions from the ground state to the additional $^4F_{9/2}$, $^4F_{7/2}$, and $^4I_{9/2}$ states, respectively.[29]

To evaluate the photocatalytic activity of the Er^{3+} doped g-C_3N_4, the degradation of Rhodamine B (RhB) was chosen as the model reaction and a blue LED (465 nm) was used as the light source. The 465 nm light is able to trigger the excitation of Er^{3+} so that to evaluate the effects of doping treatment.[26,30] Figure 2b shows the photodegradation of RhB in the presence of the Er^{3+} doped g-C_3N_4 with different doping levels. The photoactivity of the Er^{3+}-doped g-C_3N_4 improves with Er^{3+} concentration, and optimized performance is reached when 2%

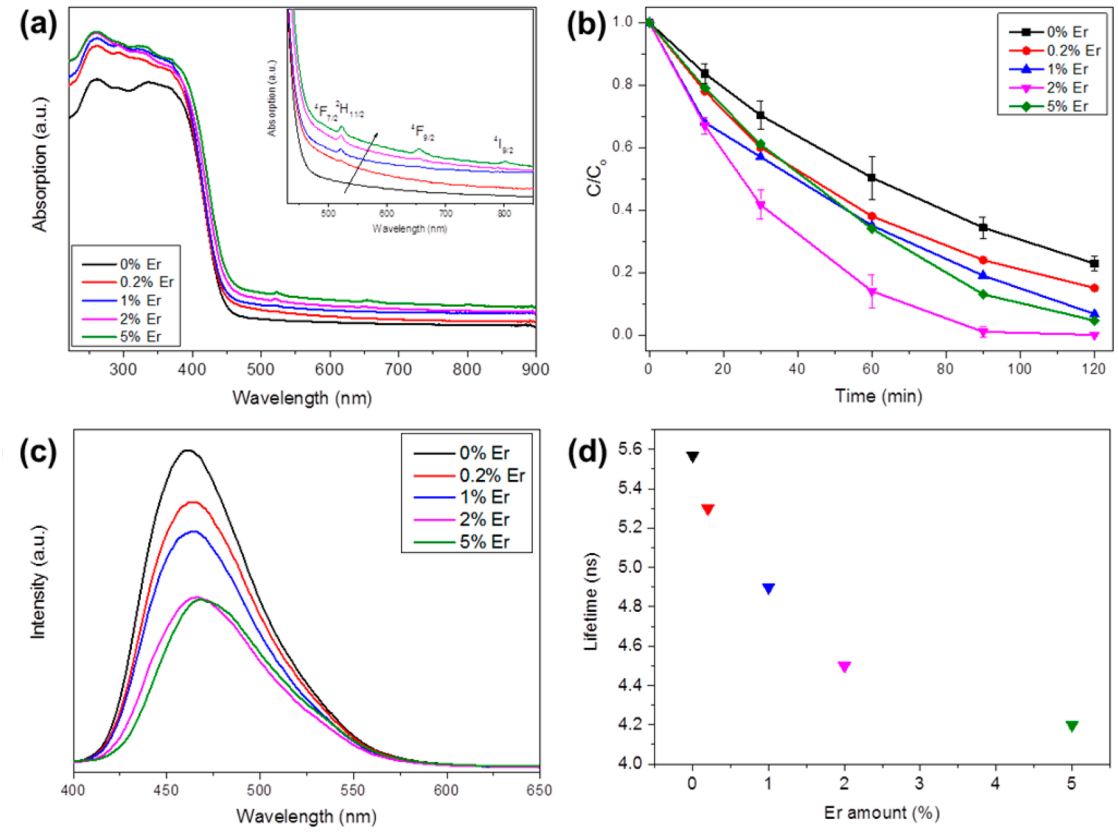

Figure 2. (a) UV−vis absorption spectra of g-C_3N_4 with different Er^{3+} doping amount. Inset: zoomed-in figure and energy transitions of ground state to the corresponding states, (b) RhB photodegradation rates over g-C_3N_4 with different Er^{3+} doping concentration at illumination wavelength of 465 nm, (c) photoluminescence spectra excited at 350 nm and (d) lifetime of g-C_3N_4 with different Er^{3+} doping amount excited at 405 nm, and with the emission monitored at 475 nm.

Er^{3+} was used, leading to complete photodegradation of RhB in 90 min, while the pristine g-C_3N_4 shows apparently less RhB degradation (~60% after 90 min). In the case of a higher Er^{3+} concentration (5%), the photoactivity starts to drop, probably because of self-quenching and/or concentration quenching of Er^{3+} as well as precipitation of crystalline $ErCl_3$ (see Table S1 in the Supporting Information).

Figure 2c shows the photoluminescence (PL) spectra of the Er^{3+}-doped g-C_3N_4 under an excitation wavelength of 350 nm. The emission intensity of the g-C_3N_4 samples peaks at 460 nm and decreases with increasing Er^{3+} concentration. It has been well established that the intensity of luminescence is closely related to the photocatalytic activity of the semiconductor,[22,31,32] and weaker band−band PL can indicate better activity of the photocatalyst.[33] Figure 2d shows the lifetime of the Er^{3+}-doped g-C_3N_4, which proves the quenching when a larger amount of Er^{3+} is present. The drop of luminescence intensity together with the lifetime reduction indicates that more photoexcited electron−hole pairs relax through a nonradiative pathway, probably by charge transfer of electrons or holes to defect states originating from rare-earth ion doping or the rare earth metal as such. Herein, the PL intensities and lifetime demonstrate a clear trend and can be a strong indicator of the photocatalytic activities of g-C_3N_4.

Several reasons accounting for the enhancement of g-C_3N_4 photocatalytic activity can be considered. Generally, the Er^{3+} ions can be excited to high energy levels by the blue light of 465 nm.[30] Then upconversion is triggered either by excited state absorption (ESA) or energy transfer (ET). ESA means that Er^{3+} in the excitation state can still absorb photon(s) to transit to higher energy levels, whereas ET refers to the energy exchange between two excited Er^{3+} ions such that one is excited into a higher lying energetic state and the other one loses its energy. Afterward upconversion luminescence would be generated when Er^{3+} ions relax to the ground state and photon energy is transferred to g-C_3N_4 and produces electron−hole pairs. This effect is expected to be responsible for the photoactivity improvement of Er^{3+}-doped g-C_3N_4. Furthermore, it is also possible that the doping of Er^{3+} results in new defects/surface states in g-C_3N_4 and thus creates new charge-transfer paths that enhance the charge separation process and the hole/electron concentration on the surface. Then the holes are capable of oxidizing RhB directly or generate OH radicals, whereas electrons can be trapped by adsorbed oxygen molecules (e.g., at the metal ion centers), and the resulting superoxide radicals are highly active to degrade organic molecules. There are two pathways for the photodegradation of RhB. One is the cleavage of the all-conjugated structure, with the main absorption peak (~554 nm) shrinking, whereas the location does not shift; the other one is de-ethylation at the nitrogen, which features the blue-shift of the absorption peak to 498 nm.[34] Figure S5 in the Supporting Information shows the absorption spectrum of RhB solution at different time intervals under illumination over 2% Er^{3+}-doped g-C_3N_4, where the main peak at 554 nm gradually fades and indicates the complete structural cleavage of RhB.

To further confirm the effect of Er^{3+} doping, a white LED (λ > 420 nm) was employed as the light source to study the photodegradation rate of RhB over pristine g-C_3N_4 and 2% Er

dx.doi.org/10.1021/am5051263 | ACS Appl. Mater. Interfaces 2014, 6, 16481−16486

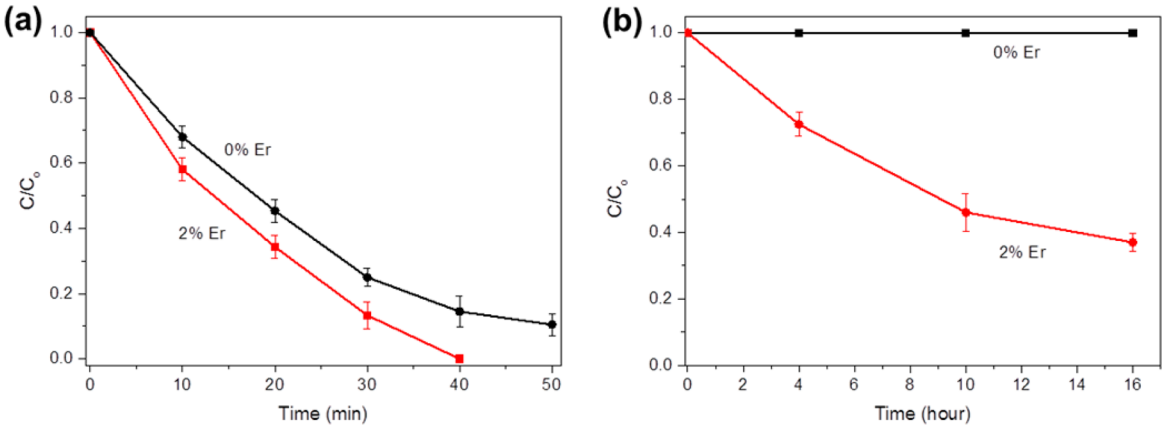

Figure 3. RhB photodegradation rates over pristine and 2% Er^{3+}-doped g-C_3N_4 under the illumination of (a) white LED and (b) red laser.

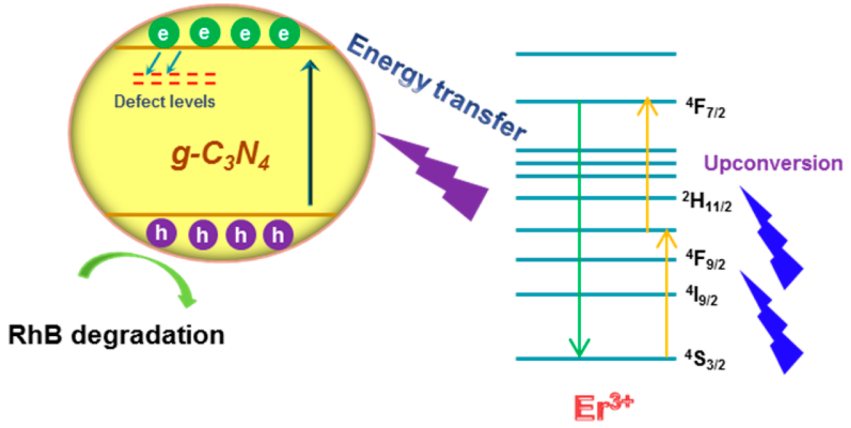

Figure 4. Schematic photodegradation mechanisms of RhB over Er^{3+}-doped g-C_3N_4.

doped g-C_3N_4. As can be seen from Figure 3a, both samples show much higher photoactivity due to the increase in the photon flux and wider spectral range. The Er^{3+}-doped g-C_3N_4 sample however clearly exhibits enhanced photoactivity, and dye degradation was completed in 40 min. To prove the upconversion contribution, we used a red laser (640−660 nm) to investigate the photocatalysis behavior. It is important to note that g-C_3N_4 does not absorb in this region, whereas the Er^{3+} has a pronounced absorption peak at 650 nm. As expected, the pristine g-C_3N_4 does not show any photoactivity, whereas more than 60% of RhB was photodegraded in the presence of 2% Er^{3+}-doped g-C_3N_4 after 16 h (Figure 3b). The photoactivity can be explained by the ability of the Er^{3+} ions for red light multiphoton absorption (Figure 2a) and transfer of these energy quanta to g-C_3N_4. It is worth pointing out that RhB dye does not degrade under red light in the absence of photocatalyst.

Importantly, we find that the surface area decreases with the Er^{3+} concentration, meaning that surface area is not responsible for the increased photoactivity (see Table S1 in the Supporting Information). This implies that changes of the electronic properties cause the improved photodegradation upon Er inclusion. We calculated the apparent reaction rate constants of RhB photodegration according to the Langmuir−Hinshelwood kinetic model,[35] which are shown in Table S1 in the Supporting Information as well as other experimental data (surface area, PL intensity, lifetimes) of the doped g-C_3N_4. This summarization clearly indicates that the enhanced photocatalytic activity of g-C_3N_4 does not result from the changing of the chemical properties, but should be attributed to the modification of optical and electronic properties via Er^{3+} doping. Consequently, we can conclude that the electronic and optical properties dominate the photocatalytic activity of the modified material. On the basis of the above results and discussions, we demonstrated possible mechanisms accounting for the enhanced photocatalytic activity of Er^{3+}-doped g-C_3N_4, mainly involving energy transfer from Er^{3+} to g-C_3N_4, as well as localized energy levels in g-C_3N_4 induced by Er^{3+} doping, as schematically shown in Figure 4. To further evaluate the photocatalytic improvement of the modified g-C_3N_4 we measured the hydrogen production under illumination. Similar to the case of RhB photodegradation, the modified g-C_3N_4 exhibited higher rates than the pristine sample under white light illumination (87 compared to 80.2 μmol h^{-1} g^{-1}). In addition, under red light illumination, hydrogen evolution was observed only in the presence of the modified g-C_3N_4 (~1.2 μmol h^{-1} g^{-1}).

As one of another typical upconversion element, thulium (Tm) was also introduced into g-C_3N_4. Figure S6a in the Supporting Information shows that the g-C_3N_4 with controlled Tm^{3+} doping concentrations (0.6, 2, and 4%) exhibits absorptions at 685 and 792 nm because of transition of $^3F_3$−$^3H_6$ and $^3F_4$−$^3H_6$, respectively.[23] All of them showed enhanced activity over RhB degradation compared to pristine g-C_3N_4, and the 2% Tm modified g-C_3N_4 exhibits the highest activity (see Figure S6b, c in the Supporting Information) under blue LED illumination. In addition, both Er^{3+}- and Tm^{3+}-doped g-C_3N_4 are stable after the photocatalytic measurements.

dx.doi.org/10.1021/am5051263 | ACS Appl. Mater. Interfaces 2014, 6, 16481−16486

After the first degradation run, the most active materials (2% Er^{3+} and 2% Tm^{3+}-doped g-C_3N_4) were left in the solution for 1 month until they were separated and washed for the next run. As shown in Figure S7 in the Supporting Information, the recycled samples still exhibit the same activity to enable the photodegradation of RhB.

In summary, we have demonstrated that the introduction of rare-earth upconversion agents, Er^{3+} and Tm^{3+} ions in particular, improves the photocatalytic activity of graphitic carbon nitride. Photodegradation of RhB indicated the performance can be optimized when 2% Er or 2% Tm ions were used. Moreover, the contribution of the upconversion agent was demonstrated by the degradation under red laser light. The improvement can result from the energy transfer from the upconversion agents to g-C_3N_4, as well as additional charge transfer paths besides radiative recombination. We believe that this work describes a simple, but effective strategy to make use of low energy photons in carbon nitride photocatalysis, offering a pathway to significantly improve its photocatalytic performance.

■ ASSOCIATED CONTENT

Supporting Information

Experimental details, SEM images, UV−vis absorption evolution of RhB aqueous solution, absorption spectra and RhB photodegradation rates over Tm^{3+} doped g-C_3N_4, photoactivity of recycled g-C_3N_4, and data summarization of Er^{3+} doped g-C_3N_4. This material is available free of charge via the Internet at http://pubs.acs.org/.

■ AUTHOR INFORMATION

Corresponding Author

*E-mail: Menny.Shalom@mpikg.mpg.de.

Notes

The authors declare no competing financial interest.

■ ACKNOWLEDGMENTS

M.S. thanks “Minerva Fellowship” for financial support. T.J.K.B. thanks Helmholtz Energy Alliance (“Hybrid Photovoltaics”) for financial support.

■ REFERENCES

(1) Osterloh, F. E. Inorganic Nanostructures for Photoelectrochemical and Photocatalytic Water Splitting. *Chem. Soc. Rev.* **2013**, *42*, 2294−2320.

(2) Vinodgopal, K.; Kamat, P. V. Enhanced Rates of Photocatalytic Degradation of an Azo Dye Using SnO_2/TiO_2 Coupled Semiconductor Thin Films. *Environ. Sci. Technol.* **1995**, *29*, 841−845.

(3) Fujiwara, H.; Hosokawa, H.; Murakoshi, K.; Wada, Y.; Yanagida, S.; Okada, T.; Kobayashi, H. Effect of Surface Structures on Photocatalytic CO_2 Reduction Using Quantized CdS Nanocrystallites 1. *J. Phys. Chem. B* **1997**, *101*, 8270−8278.

(4) Dhakshinamoorthy, A.; Navalon, S.; Corma, A.; Garcia, H. Photocatalytic CO_2 Reduction by TiO_2 and Related Titanium Containing Solids. *Energy Environ. Sci.* **2012**, *5*, 9217−9233.

(5) Fujishima, A.; Rao, T. N.; Tryk, D. A. Titanium Dioxide Photocatalysis. *J. Photochem. Photobiol., C* **2000**, *1*, 1−21.

(6) Hisatomi, T.; Dotan, H.; Stefik, M.; Sivula, K.; Rothschild, A.; Gratzel, M.; Mathews, N. Enhancement in the Performance of Ultrathin Hematite Photoanode for Water Splitting by an Oxide Underlayer. *Adv. Mater.* **2012**, *24*, 2699−2702.

(7) Jia, Q. X.; Iwashina, K.; Kudo, A. Facile Fabrication of an Efficient $BiVO_4$ Thin Film Electrode for Water Splitting under Visible Light Irradiation. *Proc. Natl. Acad. Sci. U.S.A.* **2012**, *109*, 11564−11569.

(8) Kudo, A.; Miseki, Y. Heterogeneous Photocatalyst Materials for Water Splitting. *Chem. Soc. Rev.* **2009**, *38*, 253−278.

(9) Wang, X.; Maeda, K.; Thomas, A.; Takanabe, K.; Xin, G.; Carlsson, J. M.; Domen, K.; Antonietti, M. A Metal-Free Polymeric Photocatalyst for Hydrogen Production from Water under Visible Light. *Nat. Mater.* **2009**, *8*, 76−80.

(10) Zheng, Y.; Jiao, Y.; Chen, J.; Liu, J.; Liang, J.; Du, A.; Zhang, W.; Zhu, Z.; Smith, S. C.; Jaroniec, M.; Lu, G. Q.; Qiao, S. Z. Nanoporous Graphitic-C_3N_4@Carbon Metal-Free Electrocatalysts for Highly Efficient Oxygen Reduction. *J. Am. Chem. Soc.* **2011**, *133*, 20116−20119.

(11) Liang, J.; Zheng, Y.; Chen, J.; Liu, J.; Hulicova-Jurcakova, D.; Jaroniec, M.; Qiao, S. Z. Facile Oxygen Reduction on a Three-Dimensionally Ordered Macroporous Graphitic C_3N_4/Carbon Composite Electrocatalyst. *Angew. Chem., Int. Ed.* **2012**, *51*, 3892−3896.

(12) Wang, Y.; Wang, X.; Antonietti, M. Polymeric Graphitic Carbon Nitride as a Heterogeneous Organocatalyst: from Photochemistry to Multipurpose Catalysis to Sustainable Chemistry. *Angew. Chem., Int. Ed.* **2012**, *51*, 68−89.

(13) Cao, S.; Yu, J. g-C_3N_4-Based Photocatalysts for Hydrogen Generation. *J. Phys. Chem. Lett.* **2014**, *5*, 2101−2107.

(14) Liu, G.; Niu, P.; Sun, C.; Smith, S. C.; Chen, Z.; Lu, G. Q.; Cheng, H.-M. Unique Electronic Structure Induced High Photoreactivity of Sulfur-Doped Graphitic C_3N_4. *J. Am. Chem. Soc.* **2010**, *132*, 11642−11648.

(15) Zhang, J.; Zhang, G.; Chen, X.; Lin, S.; Möhlmann, L.; Dołęga, G.; Lipner, G.; Antonietti, M.; Blechert, S.; Wang, X. Co-Monomer Control of Carbon Nitride Semiconductors to Optimize Hydrogen Evolution with Visible Light. *Angew. Chem., Int. Ed.* **2012**, *51*, 3183−3187.

(16) Martha, S.; Nashim, A.; Parida, K. M. Facile Synthesis of Highly Active g-C_3N_4 for Efficient Hydrogen Production under Visible Light. *J. Mater. Chem. A* **2013**, *1*, 7816−7824.

(17) Yan, H. Soft-templating Synthesis of Mesoporous Graphitic Carbon Nitride with Enhanced Photocatalytic H_2 Evolution under Visible Light. *Chem. Commun.* **2012**, *48*, 3430−3432.

(18) Yan, S.; Lv, S.; Li, Z.; Zou, Z. Organic−Inorganic Composite Photocatalyst of g-C_3N_4 and TaON with Improved Visible Light Photocatalytic Activities. *Dalton Trans.* **2010**, *39*, 1488−1491.

(19) Cao, S.-W.; Liu, X.-F.; Yuan, Y.-P.; Zhang, Z.-Y.; Liao, Y.-S.; Fang, J.; Loo, S. C. J.; Sum, T. C.; Xue, C. Solar-to-Fuels Conversion over In_2O_3/g-C_3N_4 Hybrid Photocatalysts. *Appl. Catal., B* **2014**, *147*, 940−946.

(20) Samanta, S.; Martha, S.; Parida, K. Facile Synthesis of Au/g-C_3N_4 Nanocomposites: An Inorganic/Organic Hybrid Plasmonic Photocatalyst with Enhanced Hydrogen Gas Evolution under Visible-Light Irradiation. *ChemCatChem.* **2014**, *6*, 1453−1462.

(21) Jun, Y. S.; Lee, E. Z.; Wang, X.; Hong, W. H.; Stucky, G. D.; Thomas, A. From Melamine-Cyanuric Acid Supramolecular Aggregates to Carbon Nitride Hollow Spheres. *Adv. Funct. Mater.* **2013**, *23*, 3661−3667.

(22) Shalom, M.; Inal, S.; Fettkenhauer, C.; Neher, D.; Antonietti, M. Improving Carbon Nitride Photocatalysis by Supramolecular Preorganization of Monomers. *J. Am. Chem. Soc.* **2013**, *135*, 7118−7121.

(23) Auzel, F. Upconversion and Anti-Stokes Processes with f and d Ions in Solids. *Chem. Rev.* **2004**, *104*, 139−174.

(24) Feng, W.; Han, C.; Li, F. Upconversion-Nanophosphor-Based Functional Nanocomposites. *Adv. Mater.* **2013**, *25*, 5287−5303.

(25) Xing, H.; Zheng, X.; Ren, Q.; Bu, W.; Ge, W.; Xiao, Q.; Zhang, S.; Wei, C.; Qu, H.; Wang, Z. Computed Tomography Imaging-Guided Radiotherapy by Targeting Upconversion Nanocubes with Significant Imaging and Radiosensitization Enhancements. *Sci. Rep.* **2013**, *3*, 1751.

(26) Zhang, Z.; Wang, W.; Yin, W.; Shang, M.; Wang, L.; Sun, S. Inducing Photocatalysis by Visible Light beyond the Absorption Edge: Effect of Upconversion Agent on the Photocatalytic Activity of Bi_2WO_6. *Appl. Catal., B* **2010**, *101*, 68−73.

(27) Wang, J.; Li, R.; Zhang, Z.; Sun, W.; Xu, R.; Xie, Y.; Xing, Z.; Zhang, X. Efficient Photocatalytic Degradation of Organic Dyes over

Titanium Dioxide Coating Upconversion Luminescence Agent under Visible and Sunlight Irradiation. *Appl. Catal., A* **2008**, *334*, 227−233.
(28) Wang, X.; Chen, X.; Thomas, A.; Fu, X.; Antonietti, M. Metal-Containing Carbon Nitride Compounds: A New Functional Organic−Metal Hybrid Material. *Adv. Mater.* **2009**, *21*, 1609−1612.
(29) Rodríguez, V. D.; Tikhomirov, V. K.; Velázquez, J. J.; Shestakov, M. V.; Moshchalkov, V. V. Visible-to-UV/Violet Upconversion Dynamics in Er^{3+}-Doped Oxyfluoride Nanoscale Glass Ceramics. *Adv. Opt. Mater.* **2013**, *1*, 747−752.
(30) Feng, G.; Liu, S.; Xiu, Z.; Zhang, Y.; Yu, J.; Chen, Y.; Wang, P.; Yu, X. Visible Light Photocatalytic Activities of TiO_2 Nanocrystals Doped with Upconversion Luminescence Agent. *J. Phys. Chem. C* **2008**, *112*, 13692−13699.
(31) Li, D.; Haneda, H.; Hishita, S.; Ohashi, N. Visible-Light-Driven N-F-Codoped TiO_2 Photocatalysts. 2. Optical Characterization, Photocatalysis, and Potential Application to Air Purification. *Chem. Mater.* **2005**, *17*, 2596−2602.
(32) Mercado, C.; Seeley, Z.; Bandyopadhyay, A.; Bose, S.; McHale, J. L. Photoluminescence of Dense Nanocrystalline Titanium Dioxide Thin Films: Effect of Doping and Thickness and Relation to Gas Sensing. *ACS Appl. Mater. Interfaces* **2011**, *3*, 2281−2288.
(33) Liqiang, J.; Yichun, Q.; Baiqi, W.; Shudan, L.; Baojiang, J.; Libin, Y.; Wei, F.; Honggang, F.; Jiazhong, S. Review of Photoluminescence Performance of Nano-Sized Semiconductor Materials and its Relationships with Photocatalytic Activity. *Sol. Energy Mater. Sol. Cells* **2006**, *90*, 1773−1787.
(34) Zhuang, J.; Dai, W.; Tian, Q.; Li, Z.; Xie, L.; Wang, J.; Liu, P.; Shi, X.; Wang, D. Photocatalytic Degradation of RhB over TiO_2 Bilayer Films: Effect of Defects and Their Location. *Langmuir* **2010**, *26*, 9686−9694.
(35) Sakkas, V. A.; Arabatzis, I. M.; Konstantinou, I. K.; Dimou, A. D.; Albanis, T. A.; Falaras, P. Metolachlor Photocatalytic Degradation Using TiO_2 Photocatalysts. *Appl. Catal., B* **2004**, *49*, 195−205.